nature medicine

Regeneration and orthotopic transplantation of a bioartificial lung

Harald C Ott[1], Ben Clippinger[1], Claudius Conrad[1], Christian Schuetz[1], Irina Pomerantseva[1], Laertis Ikonomou[2], Darrell Kotton[2] & Joseph P Vacanti[1]

About 2,000 patients now await a donor lung in the United States. Worldwide, 50 million individuals are living with end-stage lung disease. Creation of a bioartificial lung requires engineering of viable lung architecture enabling ventilation, perfusion and gas exchange. We decellularized lungs by detergent perfusion and yielded scaffolds with acellular vasculature, airways and alveoli. To regenerate gas exchange tissue, we seeded scaffolds with epithelial and endothelial cells. To establish function, we perfused and ventilated cell-seeded constructs in a bioreactor simulating the physiologic environment of developing lung. By day 5, constructs could be perfused with blood and ventilated using physiologic pressures, and they generated gas exchange comparable to that of isolated native lungs. To show *in vivo* function, we transplanted regenerated lungs into orthotopic position. After transplantation, constructs were perfused by the recipient's circulation and ventilated by means of the recipient's airway and respiratory muscles, and they provided gas exchange *in vivo* for up to 6 h after extubation.

Nearly 25 million people live with chronic obstructive pulmonary disease and approximately 120,000 patients die from end-stage lung disease annually in the United States alone[1,2]. Lung transplantation remains the only definitive treatment for end-stage lung disease. As with other organs, however, the supply of donor lungs is limited. In 2005, only one out of four patients waiting for a lung underwent transplantation (United Network of Organ Sharing). Long-term outcomes of lung transplantation are further impaired both by chronic rejection and by adverse effects of immunosuppressive treatment[3]. Creation of an autologous bioartificial lung could, theoretically, bypass these problems. A functional lung engineered on demand would allow the *de novo* generation of an organ graft that could be transplanted similarly to a donor lung. Several previous approaches have been undertaken to engineer such functional lung tissue[4]. Results from the use of polymers[5], and natural materials such as collagen[6–9], Matrigel[10,11] and Gelfoam[12], demonstrate the extracellular matrix's role not only in defining the lung's architecture and physical properties[13], but also in directing pulmonary cell differentiation[14]. Adult and embryonic cell candidates have already been isolated and differentiated into pulmonary structures *in vitro* and *in vivo*[15–21]. However, creation of substantial lung tissue that can be ventilated and perfused through a patient's airway and vasculature has been limited by the inability to generate a biodegradable, highly elastic lung scaffold that reproduces the lung's complex airway, alveolar, and vascular architecture that can support gas exchange over a large surface area[4].

In an approach previously reported in heart[22], and more recently applied to liver[23], we chose to attempt perfusion decellularization of cadaveric lungs to create whole lung scaffolds with a perfusable vascular bed and with preserved airway and alveolar geometry. A recent report of successful clinical implantation of a tissue-engineered conducting airway based on an acellular matrix scaffold, despite its lesser complexity, underlines the clinical potential of this approach in the treatment of respiratory disorders[24]. We confirmed preservation of extracellular matrix composition, integrity and mechanical properties. We then repopulated decellularized rat lungs with endothelial and epithelial cells. Chronic pulmonary arterial perfusion and fluid ventilation led to the formation of functional lungs enabling ventilation, blood perfusion and gas exchange. Ultimately, we transplanted the resulting lungs in orthotopic position, connected to the recipient's vasculature and bronchial system and documented gas exchange *in vivo*.

RESULTS

Perfusion decellularization of cadaveric lungs

A low-concentration (0.1%) sodium dodecyl sulfate (SDS)-based protocol applying a physiologic perfusion pressure was found to yield acellular whole lung scaffolds (**Fig. 1a**). Histological evaluation revealed no remaining nuclei or intracellular elements in lung parenchyma, but preservation of extracellular matrix proteins (**Fig. 1b–d** and **Supplementary Fig. 1**). Perfusion decellularization did not compromise the matrix architecture of airways and vasculature (**Fig. 1b,c**). Organization of elastic fiber network into septal, axial and pleural fibers of airways and alveoli remained intact (**Fig. 1d**). On electron microscopy, basement membranes of airways, alveoli and capillary network were found to be intact, whereas cells were absent (**Fig. 1**). At this dose of SDS, scattered nuclear remnants were found

[1]Department of Surgery, Massachusetts General Hospital, Harvard Medical School, Boston, Massachusetts, USA. [2]The Pulmonary Center and Department of Medicine, Boston University School of Medicine, Boston, Massachusetts, USA. Correspondence should be addressed to H.C.O. (hott@partners.org).

Received 22 December 2009; accepted 4 July 2010; published online 13 July 2010; doi:10.1038/nm.2193

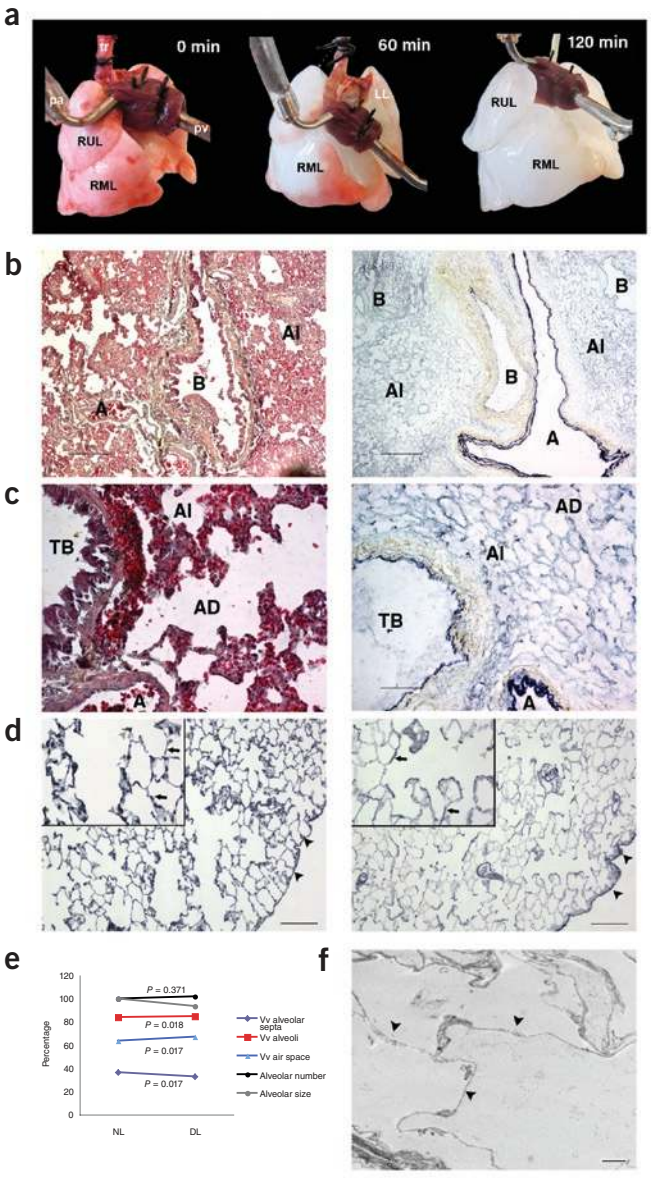

Figure 1 Perfusion decellularization of whole rat lungs. (**a**) Photographs of a cadaveric rat lung, mounted on a decellularization apparatus allowing antegrade pulmonary arterial perfusion. pa, pulmonary artery; pv, pulmonary vein; tr, trachea; RUL, right upper lobe; RML, right middle lobe; LL, left lobe. Freshly isolated lung (left), after 60 min of SDS perfusion (middle), and after 120 min of SDS perfusion (right). The lung becomes more translucent as cellular material is washed out first from apical segments, then from the middle segments and finally from the basal segments. (**b**,**c**) Corresponding Movat pentachrome staining of thin sections from parenchyma of native (left panels) and decellularized (right panels) rat lung showing preserved collagen (yellow), proteoglycans (blue) and elastic fibers (black). Low-power (top panels; scale bars, 200 μm) and high-power fields (bottom panels; scale bars, 50 μm) show preserved large (B, bronchus) and small conducting airway architecture (TB, terminal bronchus; AD, alveolar duct; AI, alveoli) and preserved large (>200 μm) and small (50 μm) arteries (A), in the absence of intact nuclei or cells in decellularized lungs. (**d**) Corresponding Verhoeff's elastic-tissue staining of thin sections from parenchyma of native (left) and decellularized (right) rat lung. Low- and high-power fields (insets) show preservation of peripheral (black arrowheads), axial (gray arrowheads) and septal (black arrows) elastic fibers in decellularized lungs. Scale bars, 200 μm. (**e**) Line chart summarizing morphometric and stereologic data from native (NL) and decellularized lungs (DL). Fractional volume (Vv) of alveolar septa decreased, whereas Vv of air space and alveoli increased with decellularization. Alveolar number expressed as percentage of that in native lung remained constant, whereas alveolar size slightly decreased (not significant). Error bars, s.d. (**f**) Transmission electron micrograph of decellularized rat lung (×6,000) showing preserved basal membranes of alveolar septa (black arrowheads) in the absence of cells or nuclei. Scale bar, 2 μm.

only within the cartilaginous rings of the trachea. Although higher concentrations of SDS (0.5%) produced complete decellularization of tracheal rings by antegrade perfusion of the thoracic aorta, we found this to compromise the integrity of membrane architecture in small vessels and alveolar septa. Hence, we selected 0.1% SDS perfusion for all subsequent experiments. This protocol led to a decrease in total DNA from 852.4 ± 161.2 ng/mg in normal lungs to 26.9 ± 13.2 ng/mg in decellularized lungs ($P = 0.011$; values expressed as mean ± s.d., throughout). Western blot analysis of decellularized lung tissue showed no residual presence of surfactant proteins, Clara cell secretory protein (CCSP; CC10) or CD31 (see below, plus data not shown). To evaluate applicability of the perfusion decellularization protocol to human-size organs, we successfully decellularized sheep, porcine and baboon lungs using a modified protocol (**Supplementary Fig. 2**).

Properties of acellular lung matrices

To compare native and decellularized lung, we applied a lung-specific histology-based morphometry and stereology protocol[25]. Consistent with cell loss, perfusion-decellularized lungs showed a decreased fractional volume of alveolar septa (32.9 ± 2.6% versus 36.3 ± 3.7%, $P = 0.017$), a correspondingly increased fractional volume of airspace (67.1 ± 2.6% versus 63.6 ± 3.7%, $P = 0.017$), and an increased fractional volume of alveolar space (88.1 ± 2.4% versus 84.0 ± 0.8%, $P = 0.018$) (**Fig. 1e**). We detected no statistically significant difference in number of alveoli measured by stereology ($16.7 \times 10^6 \pm 1.7 \times 10^6$ versus $16.4 \times 10^6 \pm 1.9 \times 10^6$, $P = 0.769$) nor size of alveoli ($2.9 \pm 0.21 \times 10^5$ μm^3 versus $3.16 \pm 0.37 \times 10^5$ μm^3, $P = 0.560$) between decellularized and native lung (**Fig. 1e**), suggesting preservation of alveolar septation and of alveolar surface area. On dynamic lung function testing, we found decellularized lungs to have relatively low compliance. Vital capacity was lower in decellularized lungs than in native lungs (13.5 ± 1.5 ml per kilogram body weight versus 35 ± 1.7 ml/kg, $P = 0.001$), as was compliance (0.27 ± 0.03 ml•cm H_2O^{-1}•s^{-1} versus 0.69 ± 0.03 ml•cm H_2O^{-1}•s^{-1}, $P = 0.001$), findings expected in decellularized lung scaffolds that lack surfactants and show pulmonary and interstitial edema when perfused before recellularization.

Recellularization of acellular lung matrices

To test whether acellular whole lung scaffolds could be repopulated with cells and maintained in organ culture, we mounted acellular rat lungs in a bioreactor designed to simulate the environment of a developing lung just before the transition to air breathing (**Supplementary Fig. 3**). In previous experiments with hearts, we found the denuded acellular vascular network of whole organ scaffolds to be incompetent and thrombogenic after transplantation[22]. We therefore attempted to repopulate acellular lung scaffolds with dsRed-labeled human umbilical cord endothelial cells (HUVECs). After 5 d of isolated organ culture, we observed dispersion of endothelial cells and engraftment throughout the scaffold, from main pulmonary artery, to lobar and segmental branches, to capillaries and pulmonary veins (**Fig. 2a**).

To test biocompatibility of scaffold, bioreactor and culture conditions, we attempted to re-epithelialize lung scaffolds with human epithelial cells. After endothelial cell seeding through the scaffold's

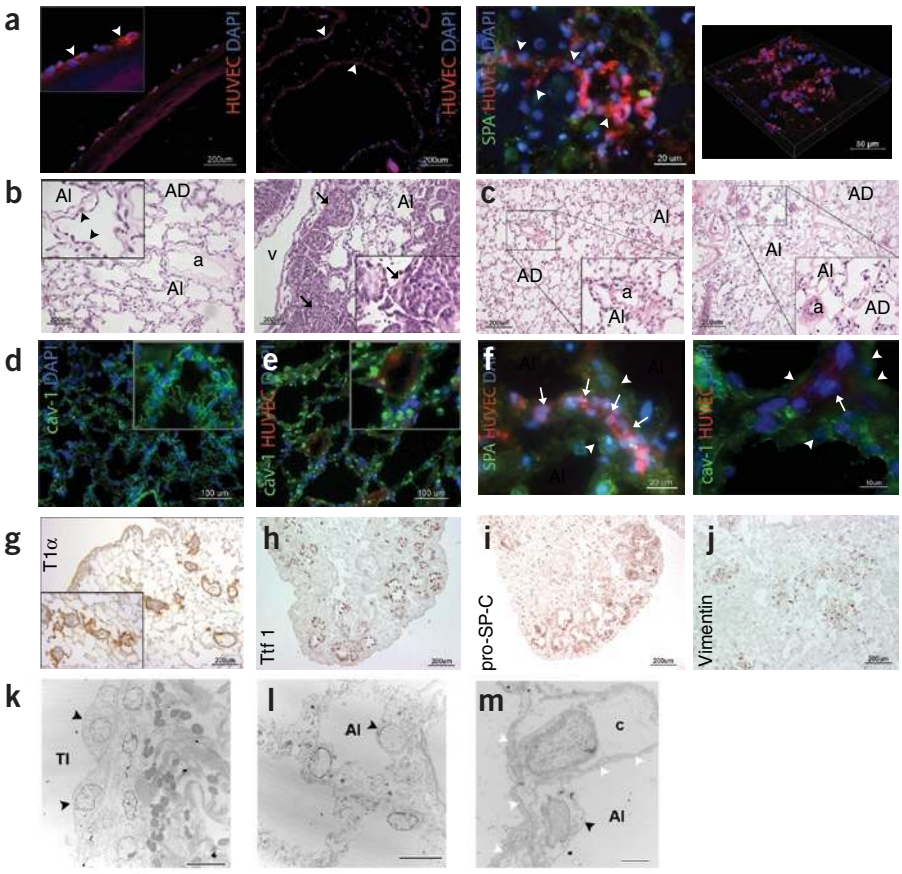

Figure 2 Histology of regenerated lung constructs. (**a**) Fluorescence micrographs of re-endothelialized lung sections (three left panels; scale bars, 200 μm) and three-dimensional reconstruction (right panel; scale bar, 50 μm). DsRed-labeled, DAPI-positive HUVECs (white arrowheads) formed a monolayer on the main pulmonary artery (first panel), segmental pulmonary arteries (a) and veins (v) (second panel) and capillaries (white arrowheads, third panel). Right, HUVEC-seeded capillary network within alveolar septa. (**b**) H&E-stained low- (×10) and high-power views (×40, insets) of A549-seeded lung constructs. Scale bars, 200 μm. a, artery; v, vein; AD, alveolar duct; Al, alveoli. A549 cells formed a complete epithelial monolayer (black arrowheads) by day 5 (left). With increased culture time (day 9, right), A549 cells formed solid tissue (black arrows) leading to obliteration of airways and alveoli. (**c**) H&E-stained low- (×10) and high-power views (×40, insets) of native lung (left) and HUVEC and FLC-seeded, regenerated lung (right). FLC and HUVEC repopulated the vascular tree and alveoli without evidence of tumor formation or airway and alveolar obliteration (day 7). (**d**) Immunofluorescence micrographs of native lung sections showing expression of caveolin-1 (cav-1) (×10, scale bar, 100 μm; inset, ×40). (**e**) Immunofluorescence micrographs of HUVEC- and FLC-seeded, regenerated lung sections showing expression of cav-1 (×10, scale bar, 100 μm; inset, ×40) and engraftment of DsRed$^+$ HUVECs. (**f**) High-power view (left, ×40, scale bar, 20 μm; right, ×80, scale bar, 10 μm) showing pneumocytes (white arrowheads) forming a single layer of cytoplasm over endothelial cell–lined capillaries (white arrows) in the alveolar septum. (**g**–**j**) Bright-field micrograph of regenerated lung section stained for T1α (brown; **g**; nuclear counterstain is methyl green), Ttf1 (brown; **h**), for pro-SPC (brown; **i**) and for vimentin (brown; **j**) showing type I pneumocytes (**g**), type II pneumocytes (**h**,**i**) and sparse fibroblasts (**j**). Scale bars, 200 μm. (**k**) Transmission electron micrograph (TEM) of regenerated rat trachea showing multilayered squamous epithelium (TI, tracheal lumen; scale bar, 10 μm). (**l**) TEM of regenerated lung showing alveolar septa repopulated with pneumocytes (black arrowhead; scale bar, 2 μm). (**m**) TEM of alveolar septum with pneumocyte (black arrowhead), endothelial cell in capillary channel (c), and intact alveolar-capillary membrane (white arrowheads; scale bar, 2 μm).

vasculature, we seeded carcinomatous human alveolar basal epithelial cells (cell line A549) delivered through the trachea. We maintained cell-seeded lung constructs for up to 9 d in isolated organ culture. The A549 cells were dispersed homogeneously, extending from large to small airways, terminal bronchioles, alveolar ducts and alveoli, using ventilation with cell culture medium. Engraftment and formation of an epithelial monolayer by culture day 5 was observed throughout the entire lung constructs, with preservation of parenchymal architecture (**Fig. 2b**, left). However, with increased culture time (>6 d), the A549 cells' lack of growth regulation and tendency to form multiple layers led to obliteration of airways, loss of surface area and, ultimately, formation of solid tissue (**Fig. 2b**, right). Despite this high cell density and thickness approximating solid tissue (>5 mm), we did not observe tissue necrosis, suggesting intact tissue perfusion by way of the vascular system.

To preserve the formation of gas exchange tissue, we next seeded decellularized cadaveric lungs with a combination of rat fetal lung cells (FLCs) and HUVECs. After re-endothelialization through the vascular system, we prepared single-cell suspensions of FLCs obtained by enzymatic digest of fetal rat lungs isolated at late canalicular development stage (gestational days 19-20). We instilled the resulting cells by means of fluid ventilation through the decellularized trachea. FLCs freshly isolated from rodents are known to consist of a heterogeneous mixture of all lung cell types, including epithelial, endothelial and interstitial lineages. When cultured on cell culture plastic for 24 h after isolation, most of the adherent portion of FLCs were found to express the type II pneumocyte–specific marker SP-C, the nonspecific epithelial and endothelial marker caveolin-1 and the pan-epithelial cell marker CK-18 (**Supplementary Fig. 4**). We cultured the reseeded whole lung constructs under physiologic conditions for up to 9 d. On histologic evaluation after 5 d in culture, we observed repopulation of the entire pulmonary scaffold with epithelial and endothelial cells, with preservation of architecture of large and small conducting airways, alveoli and vasculature (**Fig. 2c**). In contrast to the results in A549-seeded constructs, we did not observe multilayer formation, growth of solid tissue or airway obstruction. FLCs engrafted on the lung's extracellular matrix and formed regenerated epithelium in conducting airways and alveoli. Immunofluorescence staining confirmed expression of caveolin-1 as a nonspecific marker expressed in type I and II pneumocytes and endothelial cells similarly to its expression in native lung (**Fig. 2d**,**e**). At the level of alveoli and, most importantly, the alveolar septum, pneumocytes were close to endothelial cells, in a manner resembling the microanatomy of native lung (**Fig. 2f**). Within the repopulated alveolar walls we observed interspersed type II pneumocytes, confirmed by expression of surfactant proteins A

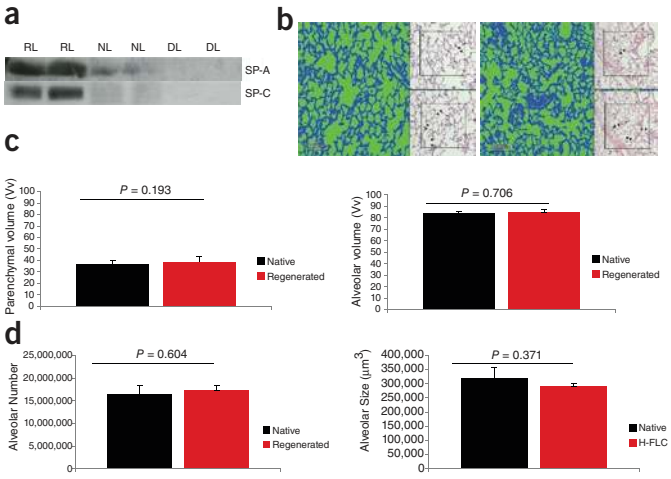

Figure 3 Protein analysis, morphometry and stereology of regenerated lung constructs. (**a**) Representative western blots of regenerated (RL), native (NL) and decellularized lung (DL) samples showing presence of surfactant proteins A (SP-A) and C (SP-C) in regenerated lung samples. (**b**) Low-power field threshold views (×10; scale bars, 200 μm) of normal lung (left) and regenerated lung (right) showing airspace in green and alveolar septa in blue. Top and bottom insets show corresponding H&E-stained views of lung sections with superimposed stereology disectors. Arrowheads mark new alveolar openings (bridges) that were counted to assess the Euler-Poincaré characteristic of the alveolar network. (**c**) Bar graphs showing fractional volume (Vv) of parenchyma (left) and alveoli (right) of native and regenerated lungs. (**d**) Bar graphs showing alveolar number and alveolar size of native and regenerated lung. Error bars, s.d..

and C (**Fig. 2**) and thyroid transcription factor-1 (Ttf1, also known as Nkx2-1). Most Ttf1$^+$ cells localized to luminal spaces bordered by rings of cuboidal cells expressing nuclear Ttf1 protein. Distinct from these spaces, we observed intermittent alveolar spaces lined with flat epithelial cells expressing the type I pneumocyte marker T1α (**Fig. 2g,h**). A few cells stained positive for vimentin, suggesting engraftment, but no overgrowth, of mesenchymal support cells (**Fig. 2j**).

The trachea and large conducting airways of regenerated constructs were lined with nonciliated, nonsecretory, squamous-appearing epithelium (**Fig. 2k**). Previous reports have found squamous epithelial coverage of regenerating airways to characterize the early response to injuries, such as exposure to naphthalene, that denude the native airway epithelium[26]. The absence of Foxj1 immunostaining in these airway epithelial cells (data not shown) further demonstrated the lack of any detectable ciliated transcriptional program activity in these squamous cells at this time point. More distal conducting airways, such as distal bronchi, were found to be lined with cuboidal-appearing epithelium. In transmission electron micrographs, alveolar septal basement membranes were seen to be repopulated with pneumocytes (**Fig. 2l**). Alveolar-capillary membranes were intact and found to range from 0.2 to 4 μm (**Fig. 2m**), suggesting the morphologic basis for an adequate diffusion capacity. To confirm pneumocyte phenotype and function, we performed western blot analyses of regenerated lung tissue. Presence of surfactant proteins A and C (SP-A, SP-C) was confirmed in FLC-seeded constructs after 5 d of *in vitro* culture (**Fig. 3a**).

Architecture of regenerated lung constructs

Morphometric analysis of regenerated lungs showed a parenchymal fractional volume equal to that of native lungs (38.9 ± 4.2% versus 36.3 ± 3.7%, $P = 0.193$) and a higher parenchymal fractional volume than that of decellularized lungs (32.8 ± 2.6%, $P = 0.006$) (**Fig. 3b–d**). Fractional volumes of alveoli in regenerated lungs did not differ from those of native lungs (84.7 ± 3.7% versus 84.0 ± 0.7%, $P = 0.706$) and were slightly lower than those of decellularized lungs (88.1 ± 2.6%, $P = 0.105$) (**Fig. 3h,i**). On stereological analysis of regenerated lungs, using the Euler-Poincaré characteristic to quantify alveoli by counting alveolar openings, the number of alveoli ($17.3 \times 10^6 \pm 1.1 \times 10^6$ versus $16.4 \times 10^6 \pm 1.9 \times 10^6$, $P = 0.604$) and the size of alveoli ($2.9 \pm 0.1 \times 10^5$ μm^3 versus $3.16 \pm 0.37 \times 10^5$ μm^3, $P = 0.371$) did not differ from those of native lungs (**Fig. 3**). Thus, repopulation of decellularized lung matrix scaffolds with endothelial and epithelial cells, and maturation in a bioreactor under physiologic conditions, led to the formation of regenerated lung tissue with physiologic-appearing alveolar volume, number and size.

In vitro function of regenerated lung constructs

The defining functional property of lung tissue is the capacity to allow gas exchange between circulating blood and inhaled air. Hence, after 5 d in whole organ culture, we switched from fluid ventilation to dry ventilation (**Supplementary Movie 1**) and tested gas exchange while regenerated lungs were perfused with human red blood cells and ventilated with 98% FiO_2 (fraction of inspired oxygen) at physiologic ventilation pressures (**Fig. 4a** and **Supplementary Movie 2**). Blood gas analyses of perfusates did not differ among the experimen-

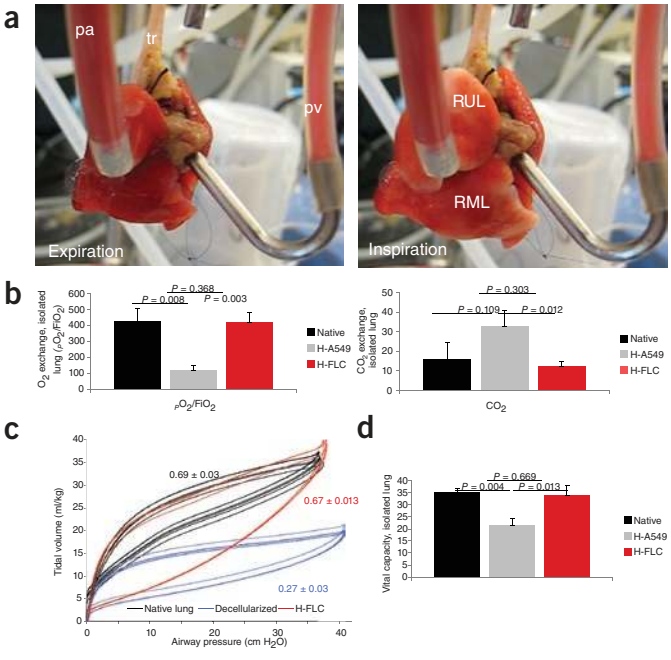

Figure 4 *In vitro* functional testing of regenerated lung constructs. (**a**) Photographs of regenerated lung constructs attached to the isolated lung apparatus (pa, pulmonary arterial cannula; pv, pulmonary venous cannula; tr, trachea) in expiration (left) and inspiration (right; RUL, right upper lobe; RML, right middle lobe). (**b**) Bar graphs showing results of blood gas analyses of pulmonary venous effluent of native lung, HUVEC- and A549-seeded lung (H-A549), and HUVEC- and fetal lung cell–seeded lung (H-FLC). Both cell-seeded lung groups showed gas exchange function; pO_2/FiO_2 ratio and pCO_2 did not differ between native and H-FLC-seeded lungs. (**c**) Line chart showing the dynamic pressure/volume relationship during five respiratory cycles of native, decellularized and regenerated lungs. Corresponding compliance values (ml/cm H_2O/s) are shown in boxes. (**d**) Bar graph comparing vital capacity of native (black), H-A549–seeded lung (gray) and H-FLC–seeded, regenerated lung (red). Error bars, s.d.

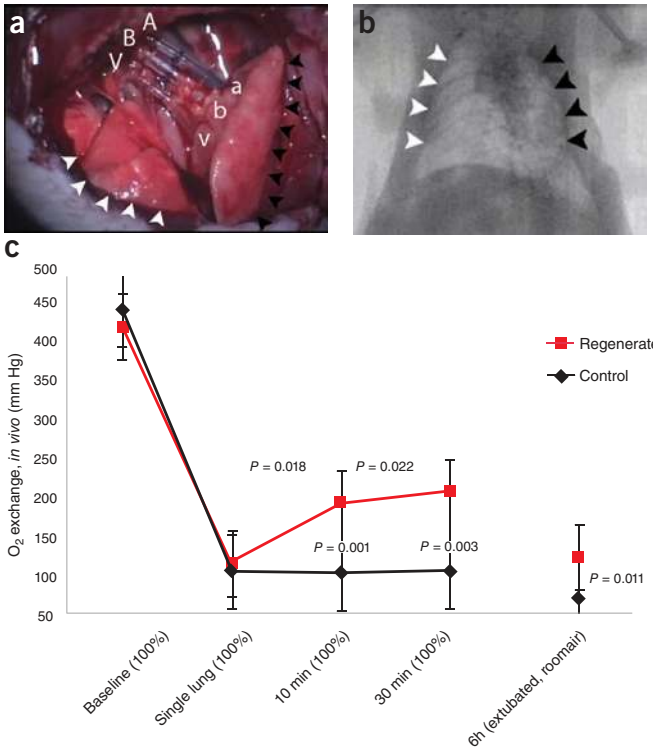

Figure 5 Orthotopic transplantation and *in vivo* function. (**a**) Photograph of left rat chest after left anterior thoracotomy, left pneumonectomy, and orthotopic transplantation of a regenerated left lung construct. Recipient left pulmonary artery (A), left main bronchus (B) and left pulmonary vein (V) are connected to regenerated left lung pulmonary artery (a), bronchus (b) and pulmonary vein (v). White arrowheads, the recipient's right lung (infracardiac and right lower lobe); back arrowheads, the regenerated left lung construct (see **Supplementary Movie 3**). (**b**) Radiograph of rat chest after left pneumonectomy and orthotopic transplantation of a regenerated left lung construct. White arrowheads, recipient's right lung; black arrowheads, regenerated left lung construct (see **Supplementary Movie 4**). (**c**) Results of blood gas analyses showing decrease in arterial oxygen tension (PaO_2) after left pneumonectomy and partial recovery after orthotopic transplantation of a regenerated left lung construct. Baseline, single lung, 10 min and 30 min measurements were obtained with the rat intubated and ventilated at volume control ventilation; 6 h measurements were obtained with the rat extubated and breathing room air without support of a ventilator. Upper *P* values compare single lung ventilation to 5 min, and 30 min time points after transplantation. Lower *P* values compare pneumonectomy to transplantation at 5 min, 30 min and 6 h time points after operation. Error bars, s.d.

tal groups (partial pressure pCO_2, 47.5 ± 8.84 mm Hg; pO_2, 49.34 ± 5.59 mm Hg; O_2 saturation, 63.7 ± 20.2%). Exchange of O_2 and CO_2 across HUVEC- and A549-seeded, regenerated lung constructs was confirmed by blood gas analysis of pulmonary venous effluents and found to be at nearly 30% of gas exchange in freshly isolated lungs (partial oxygen pressure (p_aO_2)/FiO_2 ratio, 119 ± 30; partial carbon dioxide pressure (p_aCO_2), 33 ± 8.0 mm Hg (**Fig. 4b**). Gas exchange across HUVEC- and FLC-seeded, regenerated lung constructs was significantly better and matched that in freshly isolated native lungs (p_aO_2/FiO_2 ratio, 418 ± 62 mm Hg versus 427 ± 78 mm Hg, $P = 0.368$; CO_2, 12 ± 2 mm Hg versus 16 ± 8 mm Hg, $P = 0.303$) (**Fig. 4b**). On dynamic lung function testing, HUVEC- and FLC-seeded, regenerated lungs reached a vital capacity (34 ± 3.5 ml/kg versus 35 ± 1.7 ml/kg, $P = 0.669$) and compliance (0.67 ± 0.01 ml/cm H_2O/s versus 0.69 ± 0.03 ml/cm H_2O/s, $P = 0.134$) similar to those of native lungs (**Fig. 4c**,**d**).

Orthotopic transplantation of regenerated lung constructs

Because regenerated lungs seeded with FLCs showed nearly physiologic ventilation mechanics and gas exchange capacity *in vitro*, we next sought to test whether the bioengineered lungs could function *in vivo* after orthotopic transplantation. We performed experimental left pneumonectomies and transplanted regenerated left lungs in orthotopic position. We anastomosed regenerated left lungs to the recipient's pulmonary artery, pulmonary vein and left main bronchus (**Fig. 5a** and **Supplementary Movie 3**). Ventilation and perfusion *in vivo* were documented by video recording and fluoroscopy (**Fig. 5b** and **Supplementary Movie 4**). No parenchymal bleeding, pulmonary edema or air leakage was noted from regenerated lungs in the first hour after transplant. On fluoroscopy, the regenerated lung showed radiolucency comparable to that of the native lung. As expected, blood gas analyses showed a decrease of arterial oxygen tension after left pneumonectomy in all rats (432 ± 43 mm Hg versus 118 ± 39 mm Hg; **Fig. 5c**). However, in rats that received orthotopic transplantation of regenerated lung constructs, arterial oxygen tension at 10 min and 30 min after unclamping of the pulmonary hilum improved compared to baseline (at 10 min, 199 ± 10 mm Hg versus 118 ± 39 mm Hg, $P = 0.018$; at 30 min, 214 ± 18 mm Hg versus 118 ± 39 mm Hg, $P = 0.022$) and compared to pneumonectomized control rats (at 10 min, 105 ± 10 mm Hg, $P = 0.001$; at 30 min, 108 ± 19 mm Hg, $P = 0.003$) (**Fig. 5c**). A group of rats was allowed to recover after the acute experiment, successfully extubated after transplantation and maintained without ventilatory support for 6 h after transplantation. Blood gas analyses obtained 6 h after transplantation, with the rats breathing room air, revealed significantly higher arterial blood oxygen tension in recipients of regenerated lungs compared to that in pneumonectomized controls (127 ± 18 mm Hg versus 72 ± 12 mm Hg, $P = 0.011$) (**Fig. 5c**). Over the course of several hours, the rats developed a substantial amount of nonbloody pulmonary secretions, and ultimately required reintubation before being killed as planned for graft analysis. On gross examination, vascular and bronchial anastomoses were patent, but transplanted regenerated lung constructs appeared edematous and required high inspiratory pressure (>35 cm H_2O) to be completely expanded. Histological evaluation revealed blood-perfused vasculature without evidence of interstitial hematoma, airway bleeding or thrombus formation, but with the presence of proteinaceous fluid in alveolar spaces and distal airways, suggestive of pulmonary edema.

DISCUSSION

Using a new approach, we met several milestones toward regeneration of a viable, bioartificial lung, including generation of a three-dimensional scaffold by means of perfusion-decellularization of cadaveric lung, reseeding of endothelial and epithelial surfaces of the scaffold and functional participation in gas exchange of the resulting graft both *in vitro* and *in vivo*. The successful orthotopic transplantation of a bioengineered lung in an air-breathing mammal implies that our approach may result in the *de novo* generation of either lobes or whole lungs in the future for clinical use in humans with end-stage lung diseases. To demonstrate that this technology may be scalable to human size, we decellularized ovine, porcine and primate lungs (**Supplementary Fig. 2**).

For this initial proof of concept, we chose to use a combination of HUVECs and rat FLCs from the canalicular development period (embryonic days 19–20). This stage seemed most suitable because type II pneumocytes are present but have not yet formed mature alveoli. We found cells of this particular developmental stage suitable

for regenerative experiments because of their commitment to a pneumocyte phenotype but their preservation of response to matrix-mediated growth stimulation[27]. Alternative cell populations for reseeding our scaffolds, such as derivatives of embryonic stem cells[28], induced pluripotent stem cells[29] or purified native lung epithelial populations[18], may result in more durable grafts with better *in vivo* functional capacity. As an alternative to committed lung cells, more immature cells could be seeded onto acellular lung scaffolds, relying on matrix signaling and growth factor stimulation to support pulmonary differentiation[30].

To facilitate tissue maturation, we designed a bioreactor system that subjects acellular lung scaffolds to mechanical stretch similar to that imposed by normal fetal circulation and breathing movements, necessary components of fetal lung growth and development[31]. Within 5 d in isolated organ culture, seeded cells engrafted on acellular lung scaffolds, formed endothelium and formed rudimentary respiratory and alveolar epithelium. Most importantly, recellularization and isolated organ culture led to reestablishment of an intact alveolar-capillary barrier of physiologic thickness, regenerating the morphologic basis of gas exchange[5,32]. Number and size of alveoli as functional units did not differ from those of native lung. *In vitro* ventilation and blood perfusion confirmed physiologic ventilatory mechanics and gas exchange capacity.

Orthotopic transplantation of regenerated lungs requires physiologic size, shape, airway and vascular structures, and mechanical properties that allow ventilation by means of the recipient's respiratory muscles. After cell seeding of acellular lung scaffolds and tissue maturation *in vitro*, we successfully transplanted regenerated left lung constructs after experimental left pneumonectomy. Regenerated lungs were perfused through the recipient's pulmonary artery and vein and were ventilated through the recipient's trachea. Rats could be extubated after transplantation and breathed room air without the support of a ventilator. The observed development of pulmonary secretions and interstitial edema may be related to lack of lymphatic drainage, capillary leak of immature vessels, and ventilation trauma[33,34].

Several steps will now need to be optimized to further develop our approach. Differentiation and maturation of cells in the reseeded graft will need to be improved. Although we observed encouraging signs of engraftment and differentiation of the endothelial and epithelial cells infused into our scaffolds, we also observed signs of incomplete regeneration, such as the presence of squamous epithelium, rather than ciliated or secretory cells, lining the large conducting airways. In addition, the presence of parenchymal regions lacking surfactant or T1α staining implies that some alveolar regions were not yet regenerated to maturity. Some regions of $Ttf1^+$ cuboidal epithelium in the parenchyma appeared reminiscent of type II cell hyperplasia, seen in a variety of alveolar injury-repair responses. In future work, assessment of whether these areas include clonal, multipotent and proliferative responses indicating regeneration by progenitor-like epithelial cells will be important and informative. In addition, more prolonged time in culture in our bioreactor before transplantation may yield further maturation of both parenchymal and airway regions, resulting in lung tissue that is even closer in appearance and function to native lung grafts. In addition to choice of cells, differentiation and maturation strategies, optimal graft procurement and ideal postoperative ventilation regimen of regenerated lungs will have to be developed. Future experiments will show how much *in vitro* maturation is necessary before successful long term transplantation can be achieved, and to what degree *in vivo* maturation and incorporation of host cells will complete the organ regeneration process.

METHODS

Methods and any associated references are available in the online version of the paper at http://www.nature.com/naturemedicine/.

Note: Supplementary information is available on the Nature Medicine website.

ACKNOWLEDGMENTS

We thank Harvard Apparatus Inc. for providing bioreactor components and, in particular, J. Consiglio, R. Zink and T. Beha for technical support. We thank J. Titus for assistance with animal surgeries and video recording. We further thank E. Bassett and D. Hoganson for their help with bioreactor parts and materials, A. Pardo for her technical support with western blots and K. Kulig for assistance with confocal microscopy. Electron microscopy was performed in the Microscopy Core of the Center for Systems Biology/Program in Membrane Biology, which is partially supported by Inflammatory Bowel Disease Grant DK43351 and Boston Area Diabetes and Endocrinology Research Center Award DK57521.This study was supported by a Faculty Development Grant provided by the Department of Surgery, Massachusetts General Hospital and by a Young Clinician Researcher Award granted by the Center for Integration of Medicine and Innovative Technology (CIMIT).

AUTHOR CONTRIBUTIONS

H.C.O. conceived, designed and oversaw all of the studies, collection of results, interpretation of the data and writing of the manuscript. He was responsible for the primary undertaking, completion and supervision of all experiments. B.C. was responsible for cell culture and preparation of cell suspensions. C.S. characterized fetal lung cells. C.C. assisted in animal surgeries. I.P. provided advice on animal protocols and histology techniques. L.I. performed immunohistochemistry. D.K. provided input on developmental aspects and reviewed and edited the manuscript. J.P.V. provided input on tissue engineering aspects and reviewed and edited the manuscript.

COMPETING FINANCIAL INTERESTS

The authors declare no competing financial interests.

Published online at http://www.nature.com/naturemedicine/.
Reprints and permissions information is available online at http://npg.nature.com/reprintsandpermissions/.

1. Anonymous. *National Health Interview Survey 1982–1996* (National Center for Health Statistics, 2004).
2. Anonymous. *Deaths: Final Data for 2002* (National Vital Statistics System, 2004).
3. Ng, C.Y., Madsen, J.C., Rosengard, B.R. & Allan, J.S. Immunosuppression for lung transplantation. *Front. Biosci.* **14**, 1627–1641 (2009).
4. Nichols, J.E., Niles, J.A. & Cortiella, J. Design and development of tissue engineered lung: Progress and challenges. *Organogenesis* **5**, 57–61 (2009).
5. Nichols, J.E. & Cortiella, J. Engineering of a complex organ: progress toward development of a tissue-engineered lung. *Proc. Am. Thorac. Soc.* **5**, 723–730 (2008).
6. Sugihara, H., Toda, S., Miyabara, S., Fujiyama, C. & Yonemitsu, N. Reconstruction of alveolus-like structure from alveolar type II epithelial cells in three-dimensional collagen gel matrix culture. *Am. J. Pathol.* **142**, 783–792 (1993).
7. Olsen, C.O., Isakson, B.E., Seedorf, G.J., Lubman, R.L. & Boitano, S. Extracellular matrix-driven alveolar epithelial cell differentiation *in vitro*. *Exp. Lung Res.* **31**, 461–482 (2005).
8. Mondrinos, M.J., Koutzaki, S., Lelkes, P.I. & Finck, C.M. A tissue-engineered model of fetal distal lung tissue. *Am. J. Physiol. Lung Cell. Mol. Physiol.* **293**, L639–L650 (2007).
9. Chen, P., Marsilio, E., Goldstein, R.H., Yannas, I.V. & Spector, M. Formation of lung alveolar-like structures in collagen-glycosaminoglycan scaffolds *in vitro*. *Tissue Eng.* **11**, 1436–1448 (2005).
10. Mondrinos, M.J. *et al.* Engineering three-dimensional pulmonary tissue constructs. *Tissue Eng.* **12**, 717–728 (2006).
11. Mondrinos, M.J. *et al.* *In vivo* pulmonary tissue engineering: contribution of donor-derived endothelial cells to construct vascularization. *Tissue Eng. Part A* **14**, 361–368 (2008).
12. Andrade, C.F., Wong, A.P., Waddell, T.K., Keshavjee, S. & Liu, M. Cell-based tissue engineering for lung regeneration. *Am. J. Physiol. Lung Cell. Mol. Physiol.* **292**, L510–L518 (2007).
13. Suki, B., Ito, S., Stamenovic, D., Lutchen, K.R. & Ingenito, E.P. Biomechanics of the lung parenchyma: critical roles of collagen and mechanical forces. *J. Appl. Physiol.* **98**, 1892–1899 (2005).
14. Coraux, C. *et al.* Embryonic stem cells generate airway epithelial tissue. *Am. J. Respir. Cell Mol. Biol.* **32**, 87–92 (2005).
15. Reynolds, S.D. *et al.* Conditional stabilization of beta-catenin expands the pool of lung stem cells. *Stem Cells* **26**, 1337–1346 (2008).
16. Cortiella, J. *et al.* Tissue-engineered lung: an in vivo and in vitro comparison of polyglycolic acid and pluronic F-127 hydrogel/somatic lung progenitor cell constructs to support tissue growth. *Tissue Eng.* **12**, 1213–1225 (2006).

17. Loi, R., Beckett, T., Goncz, K.K., Suratt, B.T. & Weiss, D.J. Limited restoration of cystic fibrosis lung epithelium in vivo with adult bone marrow-derived cells. *Am. J. Respir. Crit. Care Med.* **173**, 171–179 (2006).
18. Kim, C.F. *et al.* Identification of bronchioalveolar stem cells in normal lung and lung cancer. *Cell* **121**, 823–835 (2005).
19. Giangreco, A., Reynolds, S.D. & Stripp, B.R. Terminal bronchioles harbor a unique airway stem cell population that localizes to the bronchoalveolar duct junction. *Am. J. Pathol.* **161**, 173–182 (2002).
20. Kotton, D.N. *et al.* Bone marrow-derived cells as progenitors of lung alveolar epithelium. *Development* **128**, 5181–5188 (2001).
21. Pereira, R.F. *et al.* Cultured adherent cells from marrow can serve as long-lasting precursor cells for bone, cartilage, and lung in irradiated mice. *Proc. Natl. Acad. Sci. USA* **92**, 4857–4861 (1995).
22. Ott, H.C. *et al.* Perfusion-decellularized matrix: using nature's platform to engineer a bioartificial heart. *Nat. Med.* **14**, 213–221 (2008).
23. Uygun, B.E. *et al.* Organ reengineering through development of a transplantable recellularized liver graft using decellularized liver matrix. *Nat. Med.* **16**, 814–820 (2010).
24. Macchiarini, P. *et al.* Clinical transplantation of a tissue-engineered airway. *Lancet* **372**, 2023–2030 (2008).
25. Ochs, M. *et al.* The number of alveoli in the human lung. *Am. J. Respir. Crit. Care Med.* **169**, 120–124 (2004).
26. Park, K.S. *et al.* Transdifferentiation of ciliated cells during repair of the respiratory epithelium. *Am. J. Respir. Cell Mol. Biol.* **34**, 151–157 (2006).
27. Xu, J., Liu, M., Tanswell, A.K. & Post, M. Mesenchymal determination of mechanical strain-induced fetal lung cell proliferation. *Am. J. Physiol.* **275**, L545–L550 (1998).
28. Samadikuchaksaraei, A. *et al.* Derivation of distal airway epithelium from human embryonic stem cells. *Tissue Eng.* **12**, 867–875 (2006).
29. Kim, D. *et al.* Generation of human induced pluripotent stem cells by direct delivery of reprogramming proteins. *Cell Stem Cell* **4**, 472–476 (2009).
30. Cortiella, J. *et al.* Influence of acellular natural lung matrix on murine embryonic stem cell differentiation and tissue formation. *Tissue Eng. Part A* published online, doi:10.1089/ten.tea.2009.0730 (23 April 2010).
31. Kitterman, J.A. The effects of mechanical forces on fetal lung growth. *Clin. Perinatol.* **23**, 727–740 (1996).
32. Weibel, E.R. & Knight, B.W. A morphometric study on the thickness of the pulmonary air-blood barrier. *J. Cell Biol.* **21**, 367–396 (1964).
33. Cowan, G.M. Jr., Staub, N.C. & Edmunds, L.H., Jr. Changes in the fluid compartments and dry weights of reimplanted dog lungs. *J. Appl. Physiol.* **40**, 962–970 (1976).
34. Soccal, P.M. *et al.* Matrix metalloproteinases correlate with alveolar-capillary permeability alteration in lung ischemia-reperfusion injury. *Transplantation* **70**, 998–1005 (2000).

METHODS

Perfusion decellularization of lungs. All animal experiments were performed in accordance with animal welfare act, institutional guidelines and approved by the institutional animal care and use committee at the Massachusetts General Hospital. We anesthetized male, 12-week-old, Sprague-Dawley rats (Charles River), using 100 mg/kg ketamine (Phoenix Pharmaceutical), and 10 mg/kg xylazine (Phoenix Pharmaceutical) intraperitoneally. After systemic heparinization (American Pharmaceutical Partners) through the right femoral vein, a median sternotomy allowed for the opening of pericardium and bilateral pleural spaces. After the retrosternal fat body was removed, we transected the trachea at the thyroid cartilage and mobilized it distally to the bifurcation. We then transected the thoracic aorta and the superior and inferior caval veins. We mobilized both lungs and the heart and removed the entire organ package from the rat's chest. A custom-made, prefilled, 18-gauge stainless steel cannula inserted into the pulmonary artery allowed retrograde pulmonary arterial perfusion. We then ligated the ascending aorta and performed a left ventriculotomy to indirectly drain the pulmonary veins. Heparinized PBS (Invitrogen) at a pulmonary arterial perfusion pressure of 30 mm Hg for 15 min followed by 0.1% SDS (Invitrogen) in deionized water for 120 min served as perfusates. This was followed by 15 min of deionized water perfusion and 10 min of 1% Triton-X-100 (Sigma) in deionized water. Antibiotic-containing PBS (100 U/ml penicillin G, Gibco; 100 U/ml streptomycin, Gibco; and amphotericin B, Sigma) perfused the lungs for 72 h.

Bioreactor design and whole organ culture. The lung regeneration bioreactor was designed as a closed system that could be gas sterilized after cleaning and assembly, and had to be opened only once, at the time of organ loading. Flush solutions, perfusion media and cell suspensions could be infused through sterile access ports (Maximus, Medegen Inc.) to minimize the risk of contamination. The decellularized lung matrix was connected to a perfusion system through the pulmonary artery, the left atrium and the trachea and was placed in a sterile, water-jacketed organ chamber (Harvard Apparatus). The pulmonary artery was perfused with oxygenated medium at a temperature of 37 °C and a constant perfusion pressure of 10–15 mm Hg. The pulmonary vein was drained to an equilibration chamber (to minimize transpulmonary gradient during negative pressure ventilation), which was connected to the organ chamber, and from which medium was pumped back to the medium reservoir. During fluid ventilation, the trachea was connected to an equilibration chamber, which was filled from the medium reservoir. During gas ventilation, the trachea was connected to a chamber that warmed and humidified inhaled gas and functioned as a pneumotachometer (Harvard Apparatus). Pulmonary arterial line, organ chamber and pneumotachometer were connected to pressure sensors (Harvard Apparatus). Perfusion pressure, airway pressure, and tidal volumes were recorded with Pulmodyn software (Harvard Apparatus) installed on an IBM Thinkpad PC. Medium was circulated from the reservoir through a membrane oxygenator (Harvard Apparatus), where it was equilibrated with carbogen (5% CO_2 in room air), to a perfusion chamber and back to the reservoir. During fluid ventilation, the organ chamber was filled with medium; during air ventilation, the chamber was filled with filtered carbogen.

Cell seeding. Immediately after trypsinization, $66.57 \pm 18.22 \times 10^6$ human umbilical cord venous endothelial cells (HUVECs) were diluted in 20 ml of medium and seeded onto the acellular lung scaffold by means of gravity perfusion through the pulmonary artery and the pulmonary veins at a ratio of 4:1 ($n = 16$). Cells were allowed to attach for 60 min before pulmonary arterial perfusion was resumed. Carcinomatous human alveolar basal epithelial cells (A549, $91.25 \pm 31.72 \times 10^6$) were trypsinized, suspended in 15 ml of medium and seeded by means of gravity perfusion through the trachea ($n = 4$). Rat fetal lung cells were isolated following the procedure described above, counted, and resuspended in 15 ml of medium. A total of 308.57 ± 146.90 cells were seeded ($n = 8$). Cells were allowed to attach for 12 h before liquid ventilation was gently initiated.

Additional methods. Detailed descriptions of cell isolation, isolated lung experiments, orthotopic lung transplantation, histology, electron microscopy, morphometry and stereology can be found in the **Supplementary Methods**.